



# Spectroscopic evidence of the simultaneous participation of rhodium carbonyls and surface formate species during the CO<sub>2</sub> methanation catalyzed by ZrO<sub>2</sub>-supported Rh

Alfredo Solis-Garcia<sup>a,b</sup>, Trino A. Zepeda<sup>b</sup>, Juan C. Fierro-Gonzalez<sup>a,\*</sup>

<sup>a</sup> Departamento de Ingeniería Química, Tecnológico Nacional de México en Celaya, Av. Tecnológico y Antonio García Cubas s/n. Celaya, Guanajuato, Mexico 38010

<sup>b</sup> Centro de Nanociencias y Nanotecnología. Universidad Nacional Autónoma de México, Ensenada, B. C. 22800, Mexico.

## ARTICLE INFO

### Keywords:

Supported rhodium  
Carbon dioxide methanation  
Infrared spectroscopy  
Mass spectrometry  
Isotopic labelling

## ABSTRACT

ZrO<sub>2</sub>-supported rhodium nanoparticles prepared by impregnation of RhCl<sub>3</sub> are active for CO<sub>2</sub> methanation at temperatures above 180 °C. Infrared (IR) spectra recorded during catalysis allowed identification of Rh carbonyls and formate species bonded to the support. To verify their individual involvement in the catalysis, their transformations were investigated by IR spectra measured as a sample of ZrO<sub>2</sub>-supported Rh was treated with CO and isotopically labelled formic acid. The data indicate two coexisting reaction routes: a dissociative route in which CO<sub>2</sub> reacts on the Rh sample to give Rh carbonyls, and an associative route in which the CO<sub>2</sub> molecule is activated on the support, in the form of bicarbonate species that are hydrogenated to give formate species prior to methane formation. Our data show that labelled formates are transformed into Rh-<sup>13</sup>CO, thus connecting the dissociative and associative catalytic routes. The results indicate the existence of a dual mechanism for CO<sub>2</sub> methanation.

## 1. Introduction

An essential question that arises during the investigation of solid catalysts is which surface species, that are present under reaction conditions, participate as reaction intermediates and which are only spectators. The structural complexity of most solid catalysts and the diversity of reactions that occur on their surfaces complicate the analysis of spectroscopic data that characterizes functioning catalysts [1–3]. Thus, multiple interpretations could be derived from experimental results, giving rise to apparently contradictory reaction routes for a given chemical reaction. A good example of this issue is the CO<sub>2</sub> methanation (i.e. CO<sub>2</sub> + 4 H<sub>2</sub> → CH<sub>4</sub> + 2 H<sub>2</sub>O) catalyzed by supported metals, for which various mechanistic proposals have been advanced [4–10]. Specifically, two general routes have been proposed: in one of them, the CO<sub>2</sub> molecule is thought to react on the supported metal to give adsorbed carbon monoxide (CO<sub>(ads)</sub>) [11–16], whereas another proposal suggests that CO<sub>2</sub> reacts on the surface of the support to give surface formate species [8,17–20]. In each case, either formate or CO<sub>(ads)</sub> species are regarded as the crucial reaction intermediates [9] and evidence supporting both reaction routes typically comes from IR spectra of functioning catalysts [21–25], in which either CO<sub>(ads)</sub> or formate species are identified. However, matters become more complicated when both

surface species are observed simultaneously under reaction conditions [26–37]. It has typically been concluded that formate species are only spectators that are accumulated on the surface of supported Rh catalysts, and the metal carbonyls are regarded as the reaction intermediates [35–37].

In this work, we prepared a ZrO<sub>2</sub>-supported Rh sample that was catalytically active for CO<sub>2</sub> methanation. Both formate and CO<sub>(ads)</sub> species were identified in the functioning catalyst by infrared (IR) spectroscopy. To investigate the possible involvement of each surface species in the reaction, we deliberately adsorbed isotopically labelled formate species and unlabelled CO on the sample and investigated their individual transformations. Our data allowed us to establish that both CO<sub>(ads)</sub> and formate species participate in the catalysis by at least two reaction routes that are interconnected.

## 2. Experimental

### 2.1. Synthesis of ZrO<sub>2</sub>-supported rhodium samples

The ZrO<sub>2</sub> support was synthesized by a precipitation method. In the process, a 1 M solution of NH<sub>4</sub>OH was added dropwise to a 0.3 M solution of ZrO(NO<sub>3</sub>)<sub>2</sub> under constant stirring until the mixture reached a

\* Corresponding author.

<https://doi.org/10.1016/j.apcatb.2021.120955>

Received 19 August 2021; Received in revised form 6 November 2021; Accepted 18 November 2021

Available online 24 November 2021

0926-3373/© 2021 Elsevier B.V. All rights reserved.

pH value of 10 at room temperature. At that point, a precipitate was formed, which was then aged for 1 h, filtered and washed with deionized water. The obtained solid was dried at 120 °C and calcined at 500 °C in static air for 5 h. For the synthesis of the ZrO<sub>2</sub>-supported Rh sample, the appropriate amount of ZrO<sub>2</sub> was added to 50 mL of a 0.002 M solution of RhCl<sub>3</sub> to give a sample with a theoretical Rh loading of 1% w/w. Water from the mixture was evaporated under continuous stirring at 80 °C. The solid was dried at 120 °C for 5 h and then it was treated in flowing H<sub>2</sub> (60 mL min<sup>-1</sup>) at 250 °C for 1 h.

## 2.2. Characterization by X-ray diffraction (XRD)

XRD patterns of the bare support and the ZrO<sub>2</sub>-supported Rh sample (measured after both samples had been treated in flowing H<sub>2</sub> at 250 °C) were obtained with a PANalytical Aeris X-Ray powder diffractometer equipped with a Pixel 1D detector and Ni-filtered Cu-K $\alpha$  radiation ( $\lambda$  = 0.15418 nm). The instrument operated at 40 kV and 15 mA and the scanning was performed with a step of 0.02° s<sup>-1</sup> per step in a range of 2- $\theta$  between 20 and 80°.

## 2.3. Characterization by transmission electron microscopy (TEM)

TEM images of the ZrO<sub>2</sub>-supported Rh sample were acquired with a JEOL JEM-2100 F high resolution microscope operating at 200 kV and 154  $\mu$ A. Prior to the measurements, the sample was dispersed in isopropanol with an ultrasonic bath to form a suspension. Drops of the suspension were placed on a copper grid and the solvent was evaporated at room temperature.

## 2.4. CO<sub>2</sub> methanation catalytic measurements

The ZrO<sub>2</sub>-supported Rh sample was tested as catalyst for CO<sub>2</sub> methanation in a fixed-bed continuous-flow quartz reactor system at ambient pressure and temperatures ranging between 200 and 300 °C. For the experiments, the reactor was filled with 50 mg of catalyst, which was diluted with approximately 100 mg of  $\alpha$ -Al<sub>2</sub>O<sub>3</sub>. A reactive mixture consisting of 20% H<sub>2</sub>, 5% CO<sub>2</sub> and 75% Ar was fed to the reactor with a total flow rate of 60 mL min<sup>-1</sup>. The effluent gases from the reactor were analyzed by an on-line gas chromatograph (Agilent 7890) equipped with both FID and TCD and a HayeSep D column. The turnover frequency (TOF), defined as molecules of CH<sub>4</sub> produced per Rh atom per second was calculated at low CO<sub>2</sub> conversion values.

## 2.5. Operando IR characterization

Samples of the bare ZrO<sub>2</sub> support and ZrO<sub>2</sub>-supported Rh were characterized by IR spectroscopy with a Nicolet 6700 spectrometer equipped with a Harrick reaction chamber with ZnSe windows in diffuse reflectance mode (DRIFTS). Prior to the experiments, the samples were loaded into the cell and reduced with flowing H<sub>2</sub> (60 mL min<sup>-1</sup>) at 250 °C for 1 h, then they were cooled down to room temperature. For the CO<sub>2</sub> methanation tests, the reduced samples were exposed to the reaction mixture (15 mL min<sup>-1</sup> CO<sub>2</sub>, 60 mL min<sup>-1</sup> H<sub>2</sub>) while the temperature of the cell increased from room temperature to 300 °C at a rate of 5 °C min<sup>-1</sup>. In the process, IR spectra were recorded with a resolution of  $\pm$  4 cm<sup>-1</sup> and 256 scans per spectrum. The effluent gases from the flow/reactor DRIFT cell were analyzed with a Pfeiffer Omnistar mass spectrometer as the samples were treated in the flowing mixture of CO<sub>2</sub> and H<sub>2</sub> at increasing temperature. The changes in the intensities of the main fragments of hydrogen ( $m/e$  = 2), water ( $m/e$  = 18), methane ( $m/e$  = 16, 15, 14, 13, 12) carbon dioxide ( $m/e$  = 44, 28, 16, 12) and carbon monoxide ( $m/e$  = 29, 28, 16, 12) were monitored as a function of temperature.

## 2.6. In-situ IR characterization of ZrO<sub>2</sub>-supported Rh in the presence of <sup>12</sup>CO and/or H<sup>13</sup>CO<sub>2</sub>H.

In separate experiments, the reduced ZrO<sub>2</sub>-supported Rh sample was treated at room temperature with a flowing mixture of CO (50 mL of CO/N<sub>2</sub> (20% v/v CO)) and H<sub>2</sub> (15 mL min<sup>-1</sup>) or with one pulse of 15  $\mu$ L of H<sup>13</sup>COOH using H<sub>2</sub> (60 mL min<sup>-1</sup>) as carrier gas. Afterwards, the inlet and outlet valves of the reactor/DRIFT cell were closed and the temperature was increased gradually from room temperature to 300 °C at a rate of 5 °C min<sup>-1</sup> while IR spectra were acquired. In another experiment, a ZrO<sub>2</sub>-supported Rh sample was treated in flowing H<sub>2</sub> (60 mL min<sup>-1</sup>) at 200 °C for 1 h and then a pulse consisting of ca. 15  $\mu$ L of H<sup>13</sup>COOH and 15  $\mu$ L of CO was admitted to the cell with H<sub>2</sub> as a carrier gas. Simultaneously, IR spectra were recorded as a function of time.

## 3. Results and Discussion

### 3.1. Evidence of Rh nanoparticles dispersed on ZrO<sub>2</sub>

X-ray diffraction patterns of the bare ZrO<sub>2</sub> and the reduced ZrO<sub>2</sub>-supported Rh sample are shown in Fig. 1 A. In both cases, diffraction peaks corresponding to tetragonal and monoclinic ZrO<sub>2</sub> were observed (Fig. 1 A) [38,39], indicating the presence of both crystalline phases in the samples. The lack of diffraction peaks of Rh (or rhodium oxides) in the diffractogram of the supported Rh sample (Fig. 1 A) suggests high dispersion of the metal on the surface of the ZrO<sub>2</sub> support. This conclusion is bolstered by TEM images (Fig. 1B) showing the presence of Rh nanoparticles with an average diameter of approximately 2.5 nm.

### 3.2. CO<sub>2</sub> methanation catalyzed by ZrO<sub>2</sub>-supported Rh

The catalytic activity of the ZrO<sub>2</sub>-supported Rh sample for CO<sub>2</sub> methanation, reported as turnover frequency (TOF), is shown as an Arrhenius plot in Fig. 2. Data were acquired at low CO<sub>2</sub> conversion values (~5–10%) to satisfy differential reaction conditions in the fixed-bed continuous flow reactor. Only methane and water were formed during the experiments. The TOF values are comparable to those reported by others [14,40] under similar reaction conditions. Blank experiments performed in the presence of the bare support showed no formation of methane, indicating that Rh was necessary for catalysis.

In separate experiments, IR spectra were measured as samples of the bare support and ZrO<sub>2</sub>-supported Rh were treated in a flowing mixture of CO<sub>2</sub> and H<sub>2</sub> at increasing temperature. Fig. 3 A shows a comparison of the mass spectral signal of methane in the effluent gases from the flow reactor/DRIFT cell. No methane formation was detected in the presence of the ZrO<sub>2</sub> support, but when the same experiment was carried out with the supported Rh sample, the onset of methane formation occurred at approximately 180 °C (Fig. 3 A). The signal intensity of the mass fragment of methane increased continuously with increasing temperature until the set point was reached at 300 °C (Fig. 3 A). It should be noted that no CO was detected as a product during the experiment.

IR spectra of the supported Rh sample, recorded simultaneously during the experiment (Fig. 3B), show that two bands appeared at 1630 and 1450 cm<sup>-1</sup> with the admission of the reactive mixture at room temperature. These bands are assigned to the stretching vibration modes of bicarbonate species bonded to Zr<sup>4+</sup> sites on the support [41–43]. The formation of bicarbonate species might occur by a reaction between CO<sub>2</sub> and surface hydroxyl groups on the ZrO<sub>2</sub> support [44,45]. This conclusion is bolstered by a blank experiment in which the same IR bands were observed at room temperature when the bare support was treated in the flowing reactive mixture of CO<sub>2</sub> and H<sub>2</sub> (See Fig. S1 in Supplementary Data).

When the temperature increased to approximately 100 °C, IR spectra of the ZrO<sub>2</sub>-supported Rh sample showed a slight decrease in the intensities of the aforementioned bands and the appearance of a new band at 2035 cm<sup>-1</sup> (Fig. 3B), which is assigned to the CO stretching ( $\nu_{\text{CO}}$ )

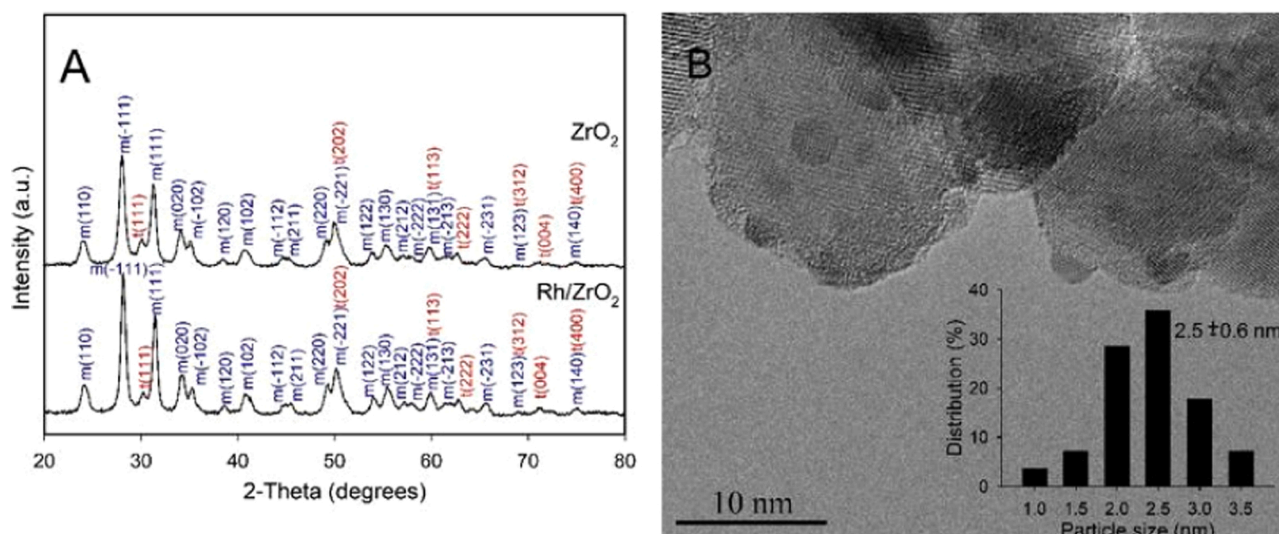


Fig. 1. (A) XRD patterns characterizing the bare  $\text{ZrO}_2$  support and a  $\text{ZrO}_2$ -supported Rh sample. (B) TEM image of a  $\text{ZrO}_2$ -supported Rh sample.

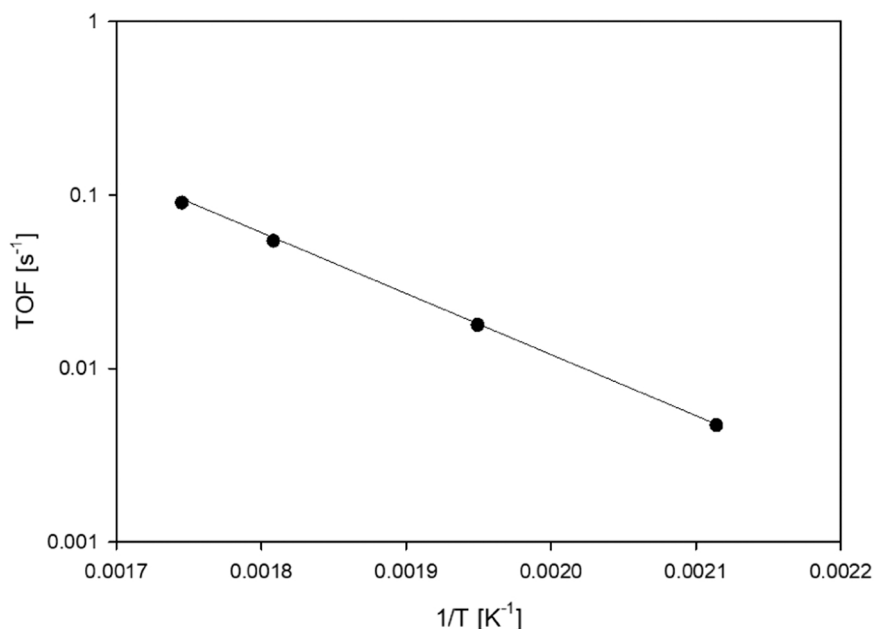
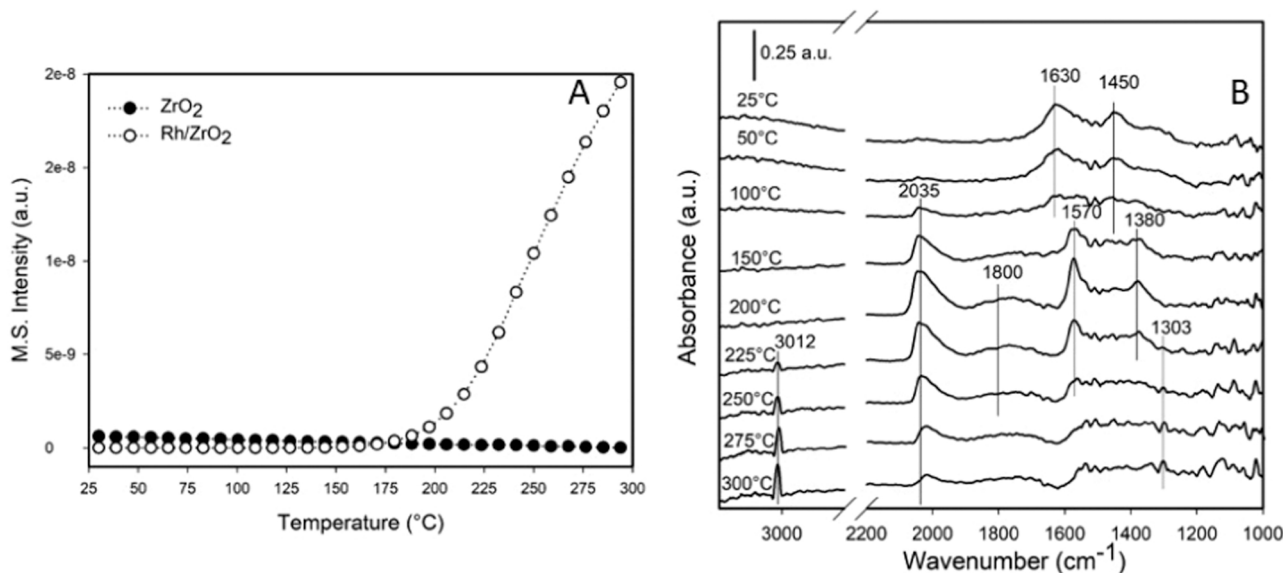


Fig. 2. Arrhenius plot of the turnover frequency of methane formation in the presence of a  $\text{ZrO}_2$ -supported Rh sample as it was treated in a flowing mixture of 20%  $\text{H}_2$ , 5%  $\text{CO}_2$  and 75% Ar at various temperatures in the range between 200 and 300 °C.

vibration mode of CO bonded to  $\text{Rh}^0$  [14,46–48]. The origin of  $\text{Rh}^0$  carbonyls on the sample could be rationalized by three separate explanations: (a) direct dissociative adsorption of  $\text{CO}_2$  on the supported Rh particles, (b) the occurrence of the reverse water-gas shift (rWGS) reaction ( $\text{CO}_2 + \text{H}_2 \rightarrow \text{CO} + \text{H}_2\text{O}$ ), and/or (c) hydrogenation of  $\text{CO}_2$ -derived surface species (e.g. bicarbonate species). There are reports of the formation of  $\text{CO}_{(\text{ads})}$  from bicarbonate species on supported rhodium [33], ruthenium [27,49,50] and palladium [29]. For instance, Heyl et al. [33] proposed that bicarbonate species bonded to  $\text{Al}_2\text{O}_3$  in  $\text{Al}_2\text{O}_3$ -supported Rh samples could be transformed into Rh carbonyls in the presence of  $\text{H}_2$  via a route in which the bicarbonate species were first hydrogenated to give formate species. However, our data do not indicate the presence of formate species at temperatures at which the  $\text{Rh}^0$  carbonyls appeared during our experiments. Thus, we can rule out the idea that the observed carbonyls at 100 °C arose from the hydrogenation of surface bicarbonate species. Regarding the possibility of rWGS reaction, it has been observed that such reaction typically occurs at temperatures

higher than 250 °C, in the presence of supported Rh catalysts [51,52]. Thus, it is unlikely that the  $\text{CO}_{(\text{ads})}$ , that was identified during the experiment at 100 °C, came from that reaction. Moreover, no gas-phase CO was observed in the effluent gases from the reactor/IR cell. Alternatively, it has been proposed that  $\text{CO}_2$  can be dissociated on the surface of metal particles to give  $\text{CO}_{(\text{ads})}$  and surface oxygen atoms [11–16]. The process is thought to occur via electron transfer from the metal to the  $\text{CO}_2$  molecule, causing cleavage of a C–O bond [53–55].  $\text{CO}_2$  dissociation has been observed, even at sub-ambient temperatures on the surfaces of various metals, including Rh [53,56], Ni [54,57–59], Ru [55], and Fe [57]. Therefore, we propose that the  $\text{Rh}^0$  carbonyls observed at 100 °C during the experiment were formed by  $\text{CO}_2$  dissociation on the supported Rh particles.

At approximately 150 °C, two bands appeared at 1570 and 1380  $\text{cm}^{-1}$  (Fig. 3B), attributed to the  $\nu\text{CO}_2$  and  $\delta\text{CH}$  vibration modes of formate species bonded to the support ( $\text{ZrO}_2$ ) [60–64]. These species might have arisen from the hydrogenation of bicarbonate species [8,



**Fig. 3.** (A) Mass spectral signal of methane ( $m/e = 15$ ) in the effluent gas from the flow reactor/DRIFT cell, measured as samples of the bare support and a ZrO<sub>2</sub>-supported Rh sample were treated in a flowing mixture of CO<sub>2</sub> and H<sub>2</sub> at increasing temperature. (B) IR spectra of the ZrO<sub>2</sub>-supported Rh sample recorded during the treatment in the flowing reactive mixture of CO<sub>2</sub>/H<sub>2</sub>.

17–20]. It is possible that H<sub>2</sub> was dissociated on the Rh particles to give hydrogen atoms that were transferred (probably via a spillover process) to the support and reacted with the bicarbonate species, as schematized in Fig. 4. In fact, the H<sub>2</sub> spillover on rhodium supported on partially reducible metal oxides has been observed even at room temperature [65–67]. Another possible explanation for the formation of formate species is the reaction between the Rh carbonyls and surface hydroxyl groups [26,50,68,69]. This possibility cannot be ruled out from the data shown in Fig. 3. IR spectra of the bare ZrO<sub>2</sub> recorded at the same conditions do not include bands of formate species (see Fig. S1 in Supplementary Data), bolstering our conclusion that those species are formed either from the hydrogenation of bicarbonate species (by hydrogen atoms that were dissociated on the Rh particles) or from Rh carbonyls.

The bands of the Rh<sup>0</sup> carbonyls and formate species increased in intensity with increasing temperature, until the ZrO<sub>2</sub>-supported Rh sample reached approximately 200 °C (Fig. 3B). At that point, a broad band appeared, centered at approximately 1800 cm<sup>-1</sup> (Fig. 3B). This band is assigned to the  $\nu_{CO}$  vibration mode of bridging CO bonded to Rh<sup>0</sup> sites [46,70–72]. Above 200 °C, the intensities of the bands of Rh<sup>0</sup> carbonyls (at 2035 and 1800 cm<sup>-1</sup>) and formate species (at 1570 and 1380 cm<sup>-1</sup>) decreased with the concomitant appearance of two bands at 3012 and 1303 cm<sup>-1</sup> (Fig. 3B). These two bands are assigned to the  $\nu_{CH}$  and  $\delta_{CH}$  vibration modes of gas-phase methane, respectively [18,19,73,74], and their appearance and increase in intensity correlates well with the rapid increase in the intensity of the mass fragment of methane, as evidenced from mass spectra of the effluent gases from the flow reactor/DRIFT cell (Fig. 3A).

In combination, the IR and mass spectral data shown in Fig. 3 suggest that the Rh<sup>0</sup> carbonyls and the surface formate species could be involved

in the CO<sub>2</sub> methanation. However, the simultaneous presence of bands of both species does not allow us to discriminate which of them are reaction intermediates or only spectators.

### 3.3. Hydrogenation of Rh<sup>0</sup> carbonyls and formate species on ZrO<sub>2</sub>-supported Rh samples

To distinguish between the possible roles of Rh<sup>0</sup> carbonyls and formate species in the CO<sub>2</sub> methanation reaction, an experiment was carried out in which the supported Rh sample was exposed deliberately to CO and isotopically labelled formate species (formed from H<sup>13</sup>CO<sub>2</sub>H) at room temperature. Then, the sample was treated under an H<sub>2</sub> atmosphere at increasing temperature and IR spectra were recorded to monitor the reactions of the various surface species. H<sup>13</sup>CO<sub>2</sub>H was selected as the probe molecule because formic acid can be adsorbed dissociatively on the surface of ZrO<sub>2</sub> to give formate species [8]. Thus, the co-adsorption of <sup>12</sup>CO and H<sup>13</sup>CO<sub>2</sub>H might allow to elucidate the individual involvement of CO(ads) and formate species in the CO<sub>2</sub> methanation by identifying the formation of <sup>12</sup>CH<sub>4</sub> and <sup>13</sup>CH<sub>4</sub>. Fig. 5 shows IR spectra of the ZrO<sub>2</sub>-supported Rh sample after admission of CO and H<sup>13</sup>CO<sub>2</sub>H to the flow reactor/DRIFT cell. At room temperature, two bands appeared at 2090 and 2023 cm<sup>-1</sup>, which are assigned to the symmetric and asymmetric CO stretching ( $\nu_a$ CO and  $\nu_s$ CO) vibration modes of dicarbonyl species bonded to Rh<sup>I</sup> [33,47,72,75]. Also, a band appeared at 1835 cm<sup>-1</sup>, attributed to bridging CO bonded to Rh<sup>0</sup> [46,70–73]. The data indicate that CO was adsorbed preferentially on the Rh particles. Conversely, five bands appeared in the region between 1550 and 1350 cm<sup>-1</sup> (Fig. 5). The bands at 1520, 1378 and 1352 cm<sup>-1</sup> can be assigned to the  $\nu_a$ (O<sup>13</sup>CO),  $\delta$ (<sup>13</sup>CH), and  $\nu_s$ (O<sup>13</sup>CO) vibration modes of

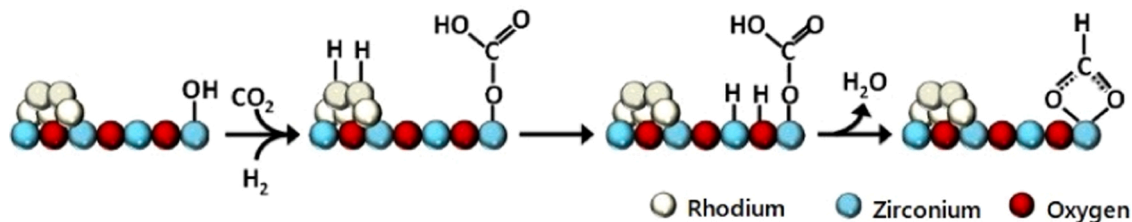


**Fig. 4.** Schematic representation of the hydrogenation of surface bicarbonate species to give formate species bonded to the support.

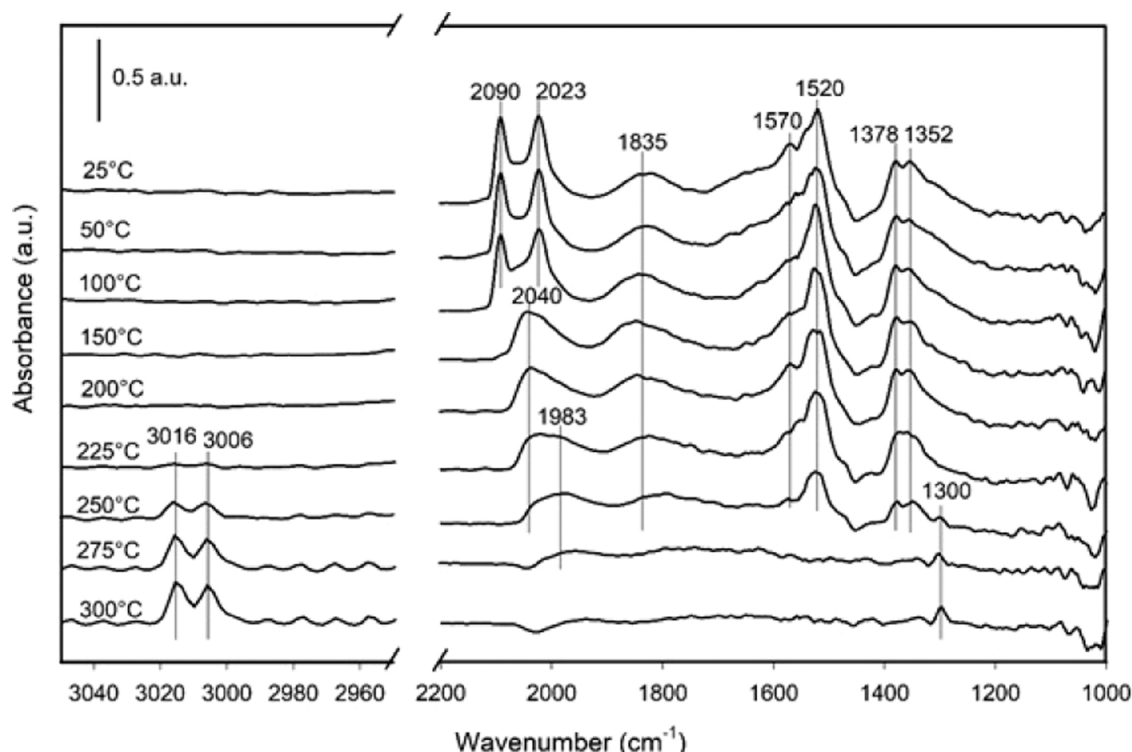


Fig. 5. IR spectra characterizing a ZrO<sub>2</sub>-supported Rh sample as it was treated in flowing H<sub>2</sub> at increasing temperature after adsorption of CO and H<sup>13</sup>CO<sub>2</sub>H at room temperature.

isotopically labelled formate species bonded to the support [76,77]. Those at 1570 and 1378 cm<sup>-1</sup> are assigned to vibration modes of unlabelled formate species [60–64]. The presence of the latter two bands was caused by impurities of unlabelled formic acid in the H<sup>13</sup>CO<sub>2</sub>H reagent. It has been reported that formic acid is dissociatively adsorbed on metal oxides by a reaction that involves surface Lewis acidic sites, leading to the formation of mono- and bi-dentate formate species [78–80]. As the temperature of the ZrO<sub>2</sub>-supported Rh sample increased under an H<sub>2</sub> atmosphere, the bands assigned to Rh<sup>I</sup> dicarbonyls decreased in intensity until they were replaced by a band at 2040 cm<sup>-1</sup> at approximately 150 °C (Fig. 5). This band is assigned to <sup>12</sup>CO linearly bonded to Rh<sup>0</sup> [46,70–72] and its appearance indicates that the rhodium was reduced from Rh<sup>I</sup> to Rh<sup>0</sup> during the H<sub>2</sub> treatment. It is noteworthy that the surface species observed during this experiment at 150 °C were analogous to those observed during the CO<sub>2</sub> methanation (Fig. 3B), namely Rh<sup>0</sup> carbonyls and formate species bonded to the ZrO<sub>2</sub> support. At temperatures higher than 200 °C (in the presence of H<sub>2</sub>), the bands attributed to rhodium carbonyls (Rh–<sup>12</sup>CO) and formate species (H<sup>13</sup>CO<sub>2</sub><sup>-</sup> and H<sup>12</sup>CO<sub>2</sub><sup>-</sup>) decreased in intensity (Fig. 5) and, at approximately 225 °C, a band appeared at 1983 cm<sup>-1</sup>. This band is assigned to <sup>13</sup>CO species bonded to Rh<sup>0</sup> (Rh–<sup>13</sup>CO) [66,81,82]. Because the only source of <sup>13</sup>C during the experiment was the isotopically labelled formic acid, it is concluded that at least some surface formate species were converted into Rh<sup>0</sup> carbonyls. A possible route for this transformation is the dehydroxylation of the formate species to give metal carbonyls and surface hydroxyl groups [70,83], as others have proposed for the CO<sub>2</sub> methanation catalyzed by Al<sub>2</sub>O<sub>3</sub>-supported Pd [29].

Concomitant with the appearance of bands of Rh carbonyls, two other bands appeared at 3016 and 3006 cm<sup>-1</sup> (Fig. 5). These bands are assigned to the ν<sub>CH</sub> vibration modes of <sup>12</sup>CH<sub>4</sub> and <sup>13</sup>CH<sub>4</sub>, respectively [18,19,73,74,84–86]. Evidence of methane is bolstered by the appearance of a band at 1300 cm<sup>-1</sup>, attributed to the δ<sub>CH</sub> vibration mode of <sup>12</sup>CH<sub>4</sub> [18,19,73,74]. Because the formation of <sup>12</sup>CH<sub>4</sub> and <sup>13</sup>CH<sub>4</sub> only occurred after Rh–<sup>13</sup>CO and Rh–<sup>12</sup>CO had been formed (and consumed), it is proposed that Rh carbonyls participate in the catalysis.

It is emphasized that Rh–<sup>13</sup>CO was formed from <sup>13</sup>C-labelled formate species on the support. Although there is a general consensus in the literature regarding the involvement of CO as an intermediate for the CO<sub>2</sub> methanation on supported Rh catalysts [13–15,87] the possible participation of formate species is still a matter of debate [33,50,88]. Our results suggest that the role of these species is to act as a reservoir to give Rh carbonyls which might, in turn, be hydrogenated to give methane.

One question that arises from the data in Fig. 5 is whether Rh carbonyls could be transformed into formate species under reaction conditions. To address this question, a sample was exposed to CO at room temperature and then treated under an H<sub>2</sub> atmosphere at increasing temperatures. IR spectra showed the appearance the ν<sub>CO</sub> bands characteristic of Rh<sup>I</sup> carbonyls at 2093 and 2025 cm<sup>-1</sup> (Fig. 6). As the temperature increased, these bands were replaced by bands of Rh<sup>0</sup> carbonyls (both linear and bridging), and their intensities decreased with the concomitant appearance of bands of methane (3014 and 1303 cm<sup>-1</sup>) at increasing temperature (Fig. 6). No bands of surface formate species were observed during the experiment. These results indicate that Rh<sup>0</sup> carbonyls are converted to methane without the involvement of formate species.

Another question that arises from the data shown in Fig. 5 is whether formate species on the ZrO<sub>2</sub>-supported Rh samples could give methane without forming CO in the process, as others have proposed on supported nickel catalysts [8,17–19,73,74]. To address this possibility, an experiment was carried out in which the ZrO<sub>2</sub>-supported Rh sample was exposed to H<sup>13</sup>CO<sub>2</sub>H at room temperature and then it was treated under an H<sub>2</sub> atmosphere at increasing temperatures. In this case, IR spectra recorded during the experiment showed the presence of labelled formate species at room temperature (Fig. 7). When the temperature increased to approximately 100 °C in the presence of H<sub>2</sub>, two new bands appeared at 1992 and 1790 cm<sup>-1</sup> (Fig. 7). The former band is assigned to the ν<sub>CO</sub> stretching mode of <sup>13</sup>CO linearly bonded to Rh<sup>0</sup> [66,81,82], whereas the latter is attributed to bridging <sup>13</sup>CO bonded to Rh<sup>0</sup> [66,81,82]. The appearance of these bands is consistent with the conclusion that part of

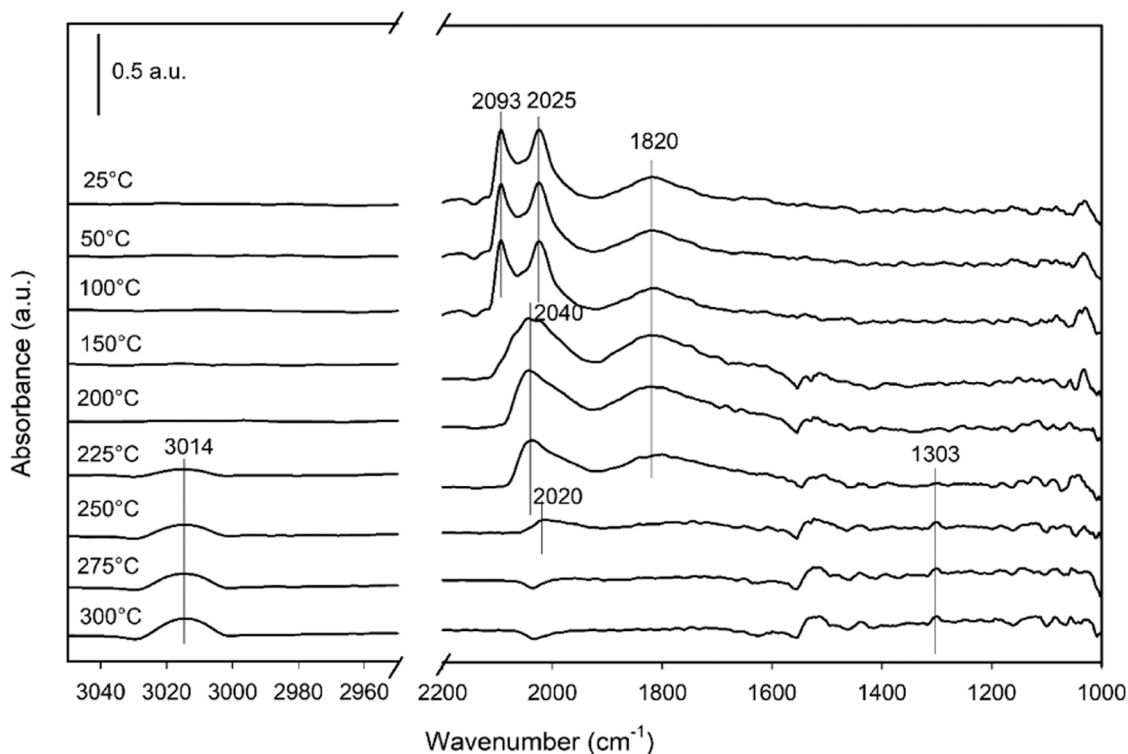


Fig. 6. IR spectra characterizing a  $\text{ZrO}_2$ -supported Rh sample as it was exposed to  $\text{H}_2$  at increasing temperature after exposure to CO at room temperature.

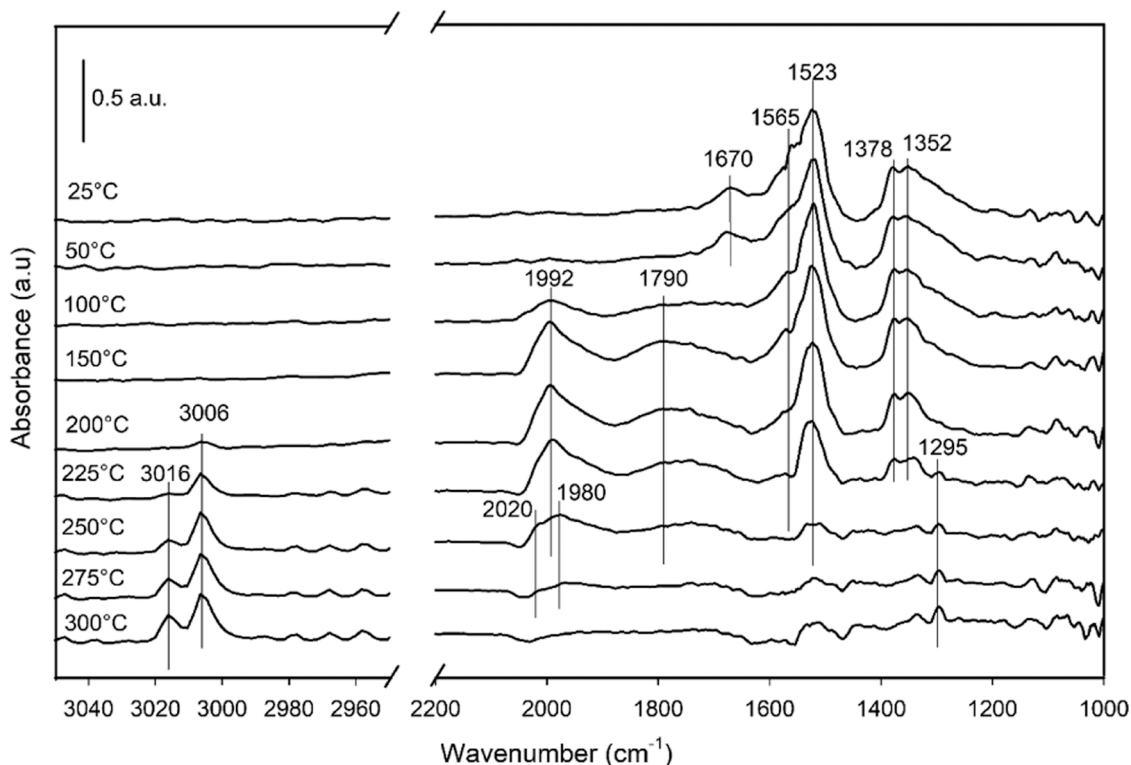


Fig. 7. IR spectra characterizing a  $\text{ZrO}_2$ -supported Rh sample as it was exposed to  $\text{H}_2$  at increasing temperature after exposure to  $\text{H}^{13}\text{CO}_2\text{H}$  at room temperature.

the initially present formate species can be transformed to  $\text{Rh}^0$  carbonyls. At temperatures higher than  $200^\circ\text{C}$ , the bands that are characteristic of carbonyl species and those of formate species decreased in intensity with the simultaneous appearance of bands at  $3006$  and  $1295\text{ cm}^{-1}$  (Fig. 7), assigned to the  $\nu_{\text{CH}}$  and  $\delta_{\text{CH}}$  vibration modes of

$^{13}\text{CH}_4$ , respectively [84–86]. A band was observed at  $3016\text{ cm}^{-1}$  and assigned to the  $\nu_{\text{CH}}$  vibration mode of  $^{12}\text{CH}_4$  [18,19,73,74].

From these data, it can be inferred that formate species could participate in the formation of methane via carbonyl species for our experimental conditions. However, the direct transformation of formate

species to methane on the support cannot be ruled out, because the decrease in the intensities of the bands of carbonyls and formate species occurs in the same temperature range. It has been proposed that formate species could be hydrogenated to methane by a route that involves methoxy [8,89] or formyl [90] species. Although we do not rule out those mechanistic routes, we do not have evidence of any of those species in IR spectra of our sample under the reaction conditions used in our experiments. Other details are also elusive to our experiments. For example, recent reports [24,91] have focused on determining whether the reactions of CO<sub>2</sub>-derived surface species during pathways involving formate species occur via C- or O-terminal hydrogenation. For that purpose, the use of theory at the density functional level in combination with experiments might be instrumental to gain further insight into those mechanistic aspects of CO<sub>2</sub> methanation.

Although the results in Fig. 5–7 indicate the involvement of CO<sub>(ads)</sub> and formate species in the catalysis, the thermal decomposition of surface formate species could also explain the decrease in the intensities of its associated bands in the spectra. To verify that possibility, a blank experiment was done in which H<sup>13</sup>CO<sub>2</sub>H was adsorbed on the bare support at room temperature and IR spectra were measured at increasing temperatures in the presence of H<sub>2</sub>. The data show a slight decrease in the intensities of the bands associated to formate species with increasing temperature (see Fig. S2 in Supplementary Data). Therefore, the decrease in the intensities of the bands of formate species in Figs. 5 and 7 is not only associated to the transformation of those species into methane, but it is also related to its thermal decomposition.

To exclude thermal effects, an experiment was done at constant temperature (200 °C) as a ZrO<sub>2</sub>-supported Rh sample was exposed to a pulse of CO and H<sup>13</sup>CO<sub>2</sub>H with flowing H<sub>2</sub> as a carrier gas. IR spectra recorded during the experiment (Fig. 8) show the appearance of bands of labelled formate species (at 1565, 1378 and 1551 cm<sup>-1</sup>), <sup>13</sup>CO<sub>(ads)</sub> (1983 cm<sup>-1</sup>) and <sup>12</sup>CO<sub>(ads)</sub> (2039 and 1835 cm<sup>-1</sup>) upon admission of the reactive mixture. Also, small bands at 3016 and 3006 cm<sup>-1</sup>, indicative of <sup>12</sup>CH<sub>4</sub> and <sup>13</sup>CH<sub>4</sub>, respectively, were identified. The latter two bands increased in intensity with increasing TOS at the expense of the bands of formate and carbonyl species (Fig. 8). After approximately 30 min in flowing H<sub>2</sub> all bands had essentially disappeared from the spectra

(Fig. 8). These results bolster the idea of coexisting mechanistic routes involving the participation of CO<sub>(ads)</sub> and formate species during the CO<sub>2</sub> methanation on the ZrO<sub>2</sub>-supported Rh catalysts.

#### 3.4. Reaction routes of CO<sub>2</sub> methanation on the surface of ZrO<sub>2</sub>-supported Rh

Based on our IR spectroscopic results, a schematic representation of the possible routes for the CO<sub>2</sub> methanation catalyzed by ZrO<sub>2</sub>-supported Rh is shown in Fig. 9. CO<sub>2</sub> can react with the surface of the sample in two different ways: (i) with surface hydroxyl groups on the support to give bicarbonate species (Fig. 9, species I) and (ii) with the supported Rh particles to form Rh carbonyls (Fig. 9, species II).

H<sub>2</sub> dissociation on the metal leads to the formation of H atoms that can react with the Rh carbonyls to form methane but some hydrogen can spillover to the support and hydrogenate the surface bicarbonate species to give formate species (Fig. 9, species III). In turn, the formate species can be further hydrogenated to produce methane. Thus, ‘dissociative’ and ‘associative’ routes coexist under the reaction conditions. In the former, CO<sub>2</sub> is dissociated to give Rh–CO as the main reaction intermediate, whereas in the latter, CO<sub>2</sub> reacts on the support to give bicarbonate species that are hydrogenated to methane via a route that involves formate species. The dissociative route involves reactions that occur exclusively on the supported metal, whereas the associative route is comprised by transformations that begin with the activation of CO<sub>2</sub> on the support. Transport of hydrogen across the metal–support interface favors the hydrogenation of CO<sub>2</sub>-derived surface species on the support to give methane. However, dehydroxylation of formate species leads to the formation of CO that can migrate from the support to the metal to give Rh carbonyls (Fig. 9). Therefore, part of the formate species connects the associative and dissociative routes, acting as a reservoir of surface CO.

#### 4. Conclusions

We investigated the CO<sub>2</sub> methanation catalyzed by ZrO<sub>2</sub>-supported Rh. Our data indicate that the sample is active at temperatures above

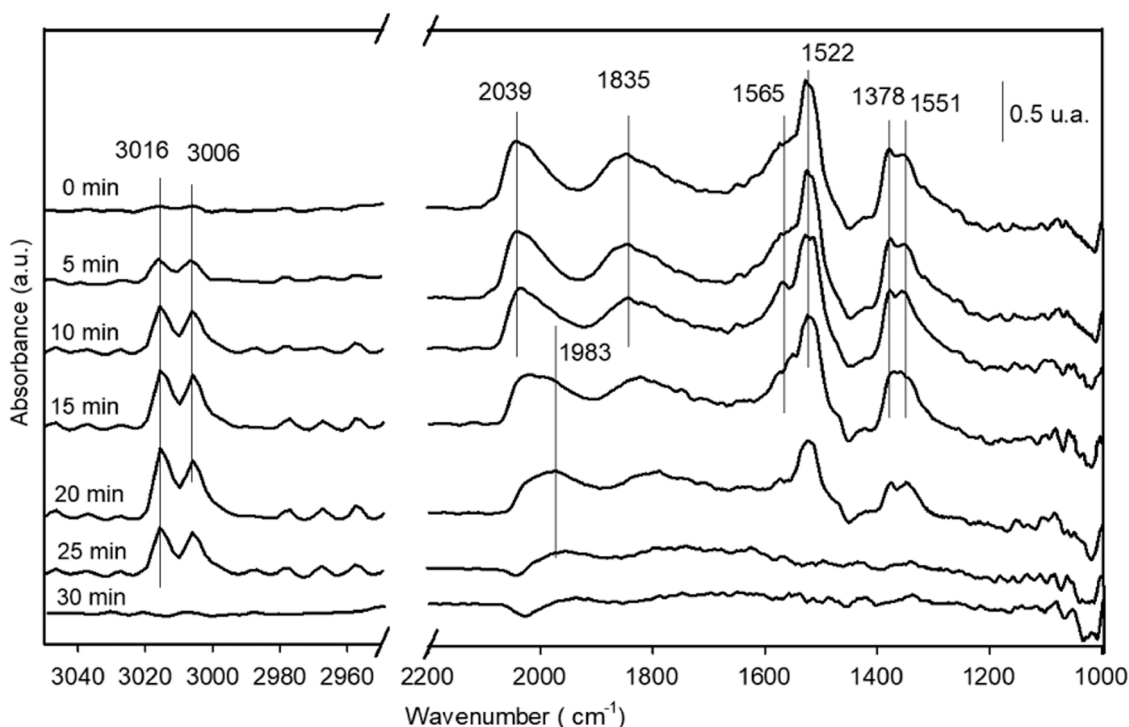


Fig. 8. IR spectra characterizing a ZrO<sub>2</sub>-supported Rh sample as it was exposed to flowing H<sub>2</sub> at 200 °C after admission of a pulse of H<sup>13</sup>CO<sub>2</sub>H and CO.

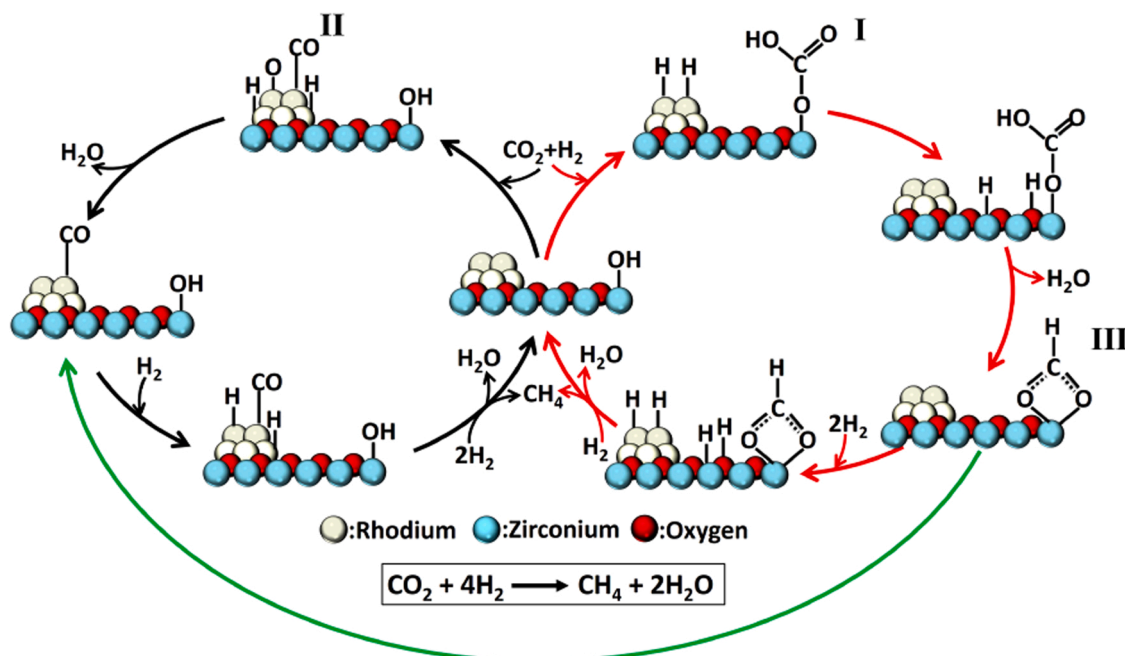


Fig. 9. Schematic representation of the proposed routes for  $\text{CO}_2$  methanation catalyzed by  $\text{ZrO}_2$ -supported Rh.

180 °C, and IR spectra characterizing the functioning catalyst allowed identification of  $\text{Rh}^0$  carbonyls and formate species on the support. The consumption of both species occurred at the same temperature range and it was concomitant with the formation of methane. Experiments were carried out to investigate the specific surface reactions of  $\text{CO}_{(\text{ads})}$  and labelled formate species with  $\text{H}_2$  on the catalyst. The data are indicative of the involvement of  $\text{CO}_{(\text{ads})}$  and formate species in two separate reaction routes that lead to methane formation.  $\text{CO}_{(\text{ads})}$  participates in a ‘dissociative’ route, in which  $\text{CO}_2$  is activated in the form of Rh carbonyls on the sample, whereas formate species (produced by an ‘associative’ route, in which  $\text{CO}_2$  reacts on the support) are either hydrogenated to give methane or transformed into  $\text{CO}$  that migrates to the supported Rh particles. Thus, part of the formate species acts as a reservoir of  $\text{CO}_{(\text{ads})}$  and connects the ‘dissociative’ and ‘associative’ routes for  $\text{CO}_2$  methanation. Our data emphasize the bifunctional character of the  $\text{ZrO}_2$ -supported Rh catalyst, showing that  $\text{CO}_2$  can be activated on both the supported Rh and on the support, whereas  $\text{H}_2$  is activated on the metal and migrates across the metal–support interface. Our results show that the surface reactions during  $\text{CO}_2$  methanation are convoluted, with the possibility of multiple reaction channels occurring simultaneously. Therefore, the reaction (apparently simple and prototypical) might not lend itself for generalizations on its mechanism. This complexity might explain the debate in the literature.

#### CRediT authorship contribution statement

**Alfredo Solis-Garcia:** Investigation, Writing – review & editing., **Trino A. Zepeda:** Writing – review & editing, Conceptualization, Visualization., **Juan C. Fierro-Gonzalez:** Writing – original draft and Editing; Conceptualization, Supervision.

#### Declaration of Competing Interest

The authors declare that they have no known competing financial interests or personal relationships that could have appeared to influence the work reported in this paper.

#### Acknowledgments

We acknowledge F. Ruiz, Y. Kotolevic and R. Yocupicio for TEM and XRD measurements. We also thank CONACYT (projects: SENER-CONACYT 117373 and Ciencia Básica 219892) and Tecnológico Nacional de México (projects: 7875.20-P and 10496.21-P) for the financial support.

#### Appendix A. Supporting information

Supplementary data associated with this article can be found in the online version at [doi:10.1016/j.apcatb.2021.120955](https://doi.org/10.1016/j.apcatb.2021.120955).

#### References

- [1] P. Serna, B.C. Gates, Molecular Metal Catalysts on Supports: Organometallic Chemistry Meets Surface Science, *Acc. Chem. Res.* 47 (2014) 2612–2620, <https://doi.org/10.1021/ar500170k>.
- [2] Y. Chen, S. Ji, C. Chen, Q. Peng, D. Wang, Y. Li, Single-Atom Catalysts: Synthetic Strategies and Electrochemical Applications, *Joule* 2 (2018) 1242–1264, <https://doi.org/10.1016/j.joule.2018.06.019>.
- [3] A. Corma, Heterogeneous Catalysis: Understanding for Designing, and Designing for Applications, *Angew. Chem. Int. Ed.* 55 (2016) 6112–6113, <https://doi.org/10.1002/anie.201601231>.
- [4] P. Frontera, A. Macario, M. Ferraro, P.L. Antonucci, Supported Catalysts for  $\text{CO}_2$  Methanation: A Review, *Catalysts* 7 (2017) 59, <https://doi.org/10.3390/catal7020059>.
- [5] M.A.A. Aziz, A.A. Jalil, S. Triwahyono, A. Ahmad,  $\text{CO}_2$  methanation over heterogeneous catalysts: recent progress and future prospects, *Green. Chem.* 17 (2015) 2647–2663, <https://doi.org/10.1039/C5GC00119F>.
- [6] E. Baraj, S. Vagaský, T. Hlinčík, K. Čiachotný, V. Tekáč, Reaction mechanisms of carbon dioxide methanation, *Chem. Pap.* 70 (2016) 395–403, <https://doi.org/10.1515/chempap-2015-0216>.
- [7] S. Rönisch, J. Schneider, S. Matthischke, M. Schlüter, M. Götz, J. Lefebvre, P. Prabhakaran, S. Bajohr, Review on methanation – From fundamentals to current projects, *Fuel* 166 (2016) 276–296, <https://doi.org/10.1016/j.fuel.2015.10.111>.
- [8] A. Solis-Garcia, J.F. Louvier-Hernandez, A. Almendarez-Camarillo, J.C. Fierro-Gonzalez, Participation of surface bicarbonate, formate and methoxy species in the carbon dioxide methanation catalyzed by  $\text{ZrO}_2$ -supported Ni, *Appl. Catal. B* 218 (2017) 611–620, <https://doi.org/10.1016/j.apcatb.2017.06.063>.
- [9] A. Solis-Garcia, J.C. Fierro-Gonzalez, Mechanistic Insights into the  $\text{CO}_2$  Methanation Catalyzed by Supported Metals: A Review, *J. Nanosci. Nanotechnol.* 19 (2019) 3110–3123, <https://doi.org/10.1166/jnn.2019.16606>.
- [10] Z. Bian, Y.M. Chan, Y. Yu, S. Kawi, Morphology dependence of catalytic properties of Ni/CeO<sub>2</sub> for  $\text{CO}_2$  methanation: A kinetic and mechanism study, *Catal. Today* 347 (2020) 31–38, <https://doi.org/10.1016/j.cattod.2018.04.067>.

- [11] J. Zheng, C. Wang, W. Chu, Y. Zhou, K. Köhler, C.O.2 Methanation, over Supported Ru/Al<sub>2</sub>O<sub>3</sub> Catalysts: Mechanistic Studies by In situ Infrared Spectroscopy, *ChemistrySelect* 1 (2016) 3197–3203, <https://doi.org/10.1002/slct.201600651>.
- [12] Z.L. Zhang, A. Kladi, X.E. Verykios, Surface Species Formed During CO and CO<sub>2</sub> Hydrogenation over Rh/TiO<sub>2</sub> (W<sup>6+</sup>) Catalysts Investigated by FTIR and Mass-Spectroscopy, *J. Catal.* 156 (1995) 37–50, <https://doi.org/10.1006/jcat.1995.1229>.
- [13] F. Solymosi, A. Erdöhelyi, T. Bánsági, Methanation of CO<sub>2</sub> on supported rhodium catalyst, *J. Catal.* 68 (1981) 371–382, [https://doi.org/10.1016/0021-9517\(81\)90106-8](https://doi.org/10.1016/0021-9517(81)90106-8).
- [14] A. Beuls, C. Swalus, M. Jacquemin, G. Heyen, A. Karellovic, P. Ruiz, Methanation of CO<sub>2</sub>: Further insight into the mechanism over Rh/ $\gamma$ -Al<sub>2</sub>O<sub>3</sub> catalyst, *Appl. Catal. B* 113 114 (2012) 2–10, <https://doi.org/10.1016/j.apcatb.2011.02.033>.
- [15] I.A. Fisher, A.T. Bell, A Comparative Study of CO and CO<sub>2</sub> Hydrogenation over Rh/SiO<sub>2</sub>, *J. Catal.* 162 (1996) 54–65, <https://doi.org/10.1006/jcat.1996.0259>.
- [16] A. Erdöhelyi, M. Pásztor, F. Solymosi, Catalytic hydrogenation of CO<sub>2</sub> over supported palladium, *J. Catal.* 98 (1986) 166–177, [https://doi.org/10.1016/0021-9517\(86\)90306-4](https://doi.org/10.1016/0021-9517(86)90306-4).
- [17] P.A.U. Aldana, F. Ocampo, K. Kobl, B. Louis, F. Thibault-Starzyk, M. Daturi, P. Bazin, S. Thomas, A.C. Roger, Catalytic CO<sub>2</sub> valorization into CH<sub>4</sub> on Ni-based ceria-zirconia. Reaction mechanism by operando IR spectroscopy, *Catal. Today* 215 (2013) 201–207, <https://doi.org/10.1016/j.cattod.2013.02.019>.
- [18] J. Ashok, M.L. Ang, S. Kawi, Enhanced activity of CO<sub>2</sub> methanation over Ni/CeO<sub>2</sub>-ZrO<sub>2</sub> catalysts: Influence of preparation methods, *Catal. Today* 281 (2017) 304–311, <https://doi.org/10.1016/j.cattod.2016.07.020>.
- [19] Q. Pan, J. Peng, S. Wang, S. Wang, In situ FTIR spectroscopic study of the CO<sub>2</sub> methanation mechanism on Ni/Ce<sub>0.5</sub>Zr<sub>0.5</sub>O<sub>2</sub>, *Catal. Sci. Technol.* 4 (2014) 502–509, <https://doi.org/10.1039/C3CY00868A>.
- [20] F. Wang, S. He, H. Chen, B. Wang, L. Zheng, M. Wei, D.G. Evans, X. Duan, Active Site Dependent Reaction Mechanism over Ru/CeO<sub>2</sub> Catalyst toward CO<sub>2</sub> Methanation, *J. Am. Chem. Soc.* 138 (2016) 6298–6305, <https://doi.org/10.1021/jacs.6b02762>.
- [21] C. Cerdá-Moreno, A. Chica, S. Keller, C. Rautenberg, U. Bentrup, Ni-sepiolite and Ni-todorokite as efficient CO<sub>2</sub> methanation catalysts: Mechanistic insight by operando DRIFTS, *Appl. Catal. B: Environ.* 264 (2020), 188546, <https://doi.org/10.1016/j.apcatb.2019.118546>.
- [22] A. Cárdenas-Arenas, A. Quindimil, A. Davó-Quinonero, E. Bailón-García, D. Lozano-Castelló, U. De-La-Torre, B. Pereda-Ayo, J.A. González-Marcos, J. R. González-Velasco, A. Bueno-López, Isotopic and in situ DRIFTS study of the CO<sub>2</sub> methanation mechanism using Ni/CeO<sub>2</sub> and Ni/Al<sub>2</sub>O<sub>3</sub> catalysts, *Appl. Catal. B: Environ.* 265 (2020), 118538, <https://doi.org/10.1016/j.apcatb.2019.118538>.
- [23] M. Hasan, T. Asakoshi, H. Muroyama, T. Matsui, K. Eguchi, CO<sub>2</sub> methanation mechanism over Ni/Y<sub>2</sub>O<sub>3</sub>: an in situ diffuse reflectance infrared Fourier transform spectroscopic study, *Phys. Chem. Chem. Phys.* 23 (2021) 5551–5558, <https://doi.org/10.1039/D0CP06257J>.
- [24] X. Xu, Y. Tong, J. Huang, J. Zhu, X. Fang, J. Xu, X. Wang, Insights into CO<sub>2</sub> methanation mechanism on cubic ZrO<sub>2</sub> supported Ni catalyst via a combination of experiments and DFT calculations, *Fuel* 283 (2021), 118867, <https://doi.org/10.1016/j.fuel.2020.118867>.
- [25] C. Liang, L. Zhang, Y. Zheng, S. Zhang, Q. Liu, G. Gao, D. Dong, Y. Wang, L. Xu, X. Hu, Methanation of CO<sub>2</sub> over nickel catalysts: Impacts of acidic/basic sites on formation of the reaction intermediates, *Fuel* 262 (2020), 116521, <https://doi.org/10.1016/j.fuel.2019.116521>.
- [26] M.A.A. Aziz, A.A. Jalil, S. Triwahyono, S.M. Sidik, Methanation of carbon dioxide on metal-promoted mesostructured silica nanoparticles, *Appl. Catal. A* 486 (2014) 115–122, <https://doi.org/10.1016/j.apcatb.2014.08.022>.
- [27] X. Wang, Y. Hong, H. Shi, J. Szanyi, Kinetic modeling and transient DRIFTS-MS studies of CO<sub>2</sub> methanation over Ru/Al<sub>2</sub>O<sub>3</sub> catalysts, *J. Catal.* 343 (2016) 185–195, <https://doi.org/10.1016/j.jcat.2016.02.001>.
- [28] A. Westermann, B. Azambre, M.C. Bacariza, I. Graça, M.F. Ribeiro, J.M. Lopes, C. Henriques, Insight into CO<sub>2</sub> methanation mechanism over NiUSY zeolites: An operando IR study, *Appl. Catal. B* 174 175 (2015) 120–125, <https://doi.org/10.1016/j.apcatb.2015.02.026>.
- [29] X. Wang, H. Shi, J.H. Kwak, J. Szanyi, Mechanism of CO<sub>2</sub> Hydrogenation on Pd/Al<sub>2</sub>O<sub>3</sub> Catalysts: Kinetics and Transient DRIFTS-MS Studies, *ACS Catal.* 5 (2015) 6337–6349, <https://doi.org/10.1021/acscatal.5b01464>.
- [30] Z. Fan, K. Sun, N. Rui, B. Zhao, C. Liu, Improved activity of Ni/MgAl<sub>2</sub>O<sub>4</sub> for CO<sub>2</sub> methanation by the plasma decomposition, 655–569, *J. Energy Chem.* 24 (2015), <https://doi.org/10.1016/j.jechem.2015.09.004>.
- [31] S.M. Lee, Y.H. Lee, D.H. Moon, J.Y. Ahn, D.D. Nguyen, S.W. Chang, S.S. Kim, Reaction Mechanism and Catalytic Impact of Ni/CeO<sub>2-x</sub> Catalyst for Low-Temperature CO<sub>2</sub> Methanation, *Ind. Eng. Chem. Res.* 58 (2019) 8656–8662, <https://doi.org/10.1021/acs.iecr.9b00983>.
- [32] L. Proano, E. Tello, M.A. Arellano-Trevino, S. Wang, R.J. Farrauto, M. Cobo, In-situ DRIFTS study of two-step CO<sub>2</sub> capture and catalytic methanation over Ru, “Na<sub>2</sub>O”/Al<sub>2</sub>O<sub>3</sub> Dual Functional Material, *Appl. Surf. Sci.* 479 (2019) 25–30, <https://doi.org/10.1016/j.apsusc.2019.01.281>.
- [33] D. Heyl, U. Rodemerck, U. Bentrup, Mechanistic Study of Low-Temperature CO<sub>2</sub> Hydrogenation over Modified Rh/Al<sub>2</sub>O<sub>3</sub> Catalysts, *ACS Catal.* 6 (2016) 6275–6284, <https://doi.org/10.1021/acscatal.6b01295>.
- [34] Y. Jiang, J. Lang, X. Wu, Y.H. Hu, Electronic structure modulating for supported Rh catalysts toward CO<sub>2</sub> methanation, *Catal. Today* 356 (2020) 570–578, <https://doi.org/10.1016/j.cattod.2020.01.029>.
- [35] S. Eckle, H.G. Anfang, R.J. Behm, Reaction Intermediates and Side Products in the Methanation of CO and CO<sub>2</sub> over Supported Ru Catalysts in H<sub>2</sub>-Rich Reformate Gases, *J. Phys. Chem. C* 115 (2011) 1361–1367, <https://doi.org/10.1021/jp108106t>.
- [36] Y. Wang, H. Arandiyán, S.A. Bartlett, A. Trunschke, H. Sun, J. Scott, A.F. Lee, K. Wilson, T. Maschmeyer, R. Schlögl, R. Amal, Inducing synergy in bimetallic RhNi catalysts for CO<sub>2</sub> methanation by galvanic replacement, *Appl. Catal. B* 277 (2020) 119029–119054, <https://doi.org/10.1016/j.apcatb.2020.119029>.
- [37] N. Schreiter, J. Kirchner, S. Kureti, A. DRIFTS and TPD study on the methanation of CO<sub>2</sub> on Ni/Al<sub>2</sub>O<sub>3</sub> catalyst, *Catal. Commun.* 140 (2020) 105988–105989, <https://doi.org/10.1016/j.catcom.2020.105988>.
- [38] F. del Monte, W. Larsen, J.D. Mackenzie, Stabilization of Tetragonal ZrO<sub>2</sub> in ZrO<sub>2</sub>-SiO<sub>2</sub> Binary Oxides, *J. Am. Ceram. Soc.* 83 (2000) 628–634, <https://doi.org/10.1111/j.1151-2916.2000.tb01243.x>.
- [39] T. Suzuki-Muresan, P. Deniard, E. Gautron, V. Petricek, S. Jobic, B. Grambow, Minimization of absorption contrast for accurate amorphous phase quantification: application to ZrO<sub>2</sub> nanoparticles, *Appl. Cryst.* 43 (2010) 1092–1099, <https://doi.org/10.1107/S0021889810032358>.
- [40] P. Panagiotopoulou, Hydrogenation of CO<sub>2</sub> over supported noble metal catalysts, *Appl. Catal. A: Gen.* 542 (2017) 63–70, <https://doi.org/10.1016/j.apcata.2017.05.026>.
- [41] M. Daturi, C. Binet, J.C. Lavalley, G. Blanchard, Surface FTIR investigations on Ce<sub>x</sub>Zr<sub>1-x</sub>O<sub>2</sub> system, *Surf. Interface Anal.* 30 (2000) 273–277, [https://doi.org/10.1002/1096-9918\(200008\)30:1<273::AID-SIA715>3.0.CO;2-G](https://doi.org/10.1002/1096-9918(200008)30:1<273::AID-SIA715>3.0.CO;2-G).
- [42] B. Bachiller-Baeza, I. Rodríguez-Ramos, A. Guerrero-Ruiz, Interaction of Carbon Dioxide with the Surface of Zirconia Polymorphs, *Langmuir* 14 (1998) 3556–3564, <https://doi.org/10.1021/la970856q>.
- [43] K. Pokrovski, K. Taek Jung, A.T. Bell, Investigation of CO and CO<sub>2</sub> Adsorption on Tetragonal and Monoclinic Zirconia, *Langmuir* 17 (2001) 4297–4303, <https://doi.org/10.1021/la001723z>.
- [44] J.C. Lavalley, Infrared spectrometric studies of the surface basicity of metal oxides and zeolites using adsorbed probe molecules, *Catal. Today* 27 (1996) 377–401, [https://doi.org/10.1016/0920-5861\(95\)00161-1](https://doi.org/10.1016/0920-5861(95)00161-1).
- [45] J. Baltrusaitis, J.H. Jensen, V.H. Grassian, FTIR Spectroscopy Combined with Isotope Labeling and Quantum Chemical Calculations to Investigate Adsorbed Bicarbonate Formation Following Reaction of Carbon Dioxide with Surface Hydroxyl Groups on Fe<sub>2</sub>O<sub>3</sub> and Al<sub>2</sub>O<sub>3</sub>, *J. Phys. Chem. B* 110 (2006) 12005–12016, <https://doi.org/10.1021/jp057437j>.
- [46] T. Chafik, D.I. Kondarides, X.E. Verykios, Catalytic Reduction of NO by CO over Rhodium Catalysts: 1. Adsorption and Displacement Characteristics Investigated by In Situ FTIR and Transient-MS Techniques, *J. Catal.* 190 (2000) 446–459, <https://doi.org/10.1006/jcat.1999.2763>.
- [47] C.A. Rice, S.D. Worley, C.W. Curtis, J.A. Guin, A.R. Tarrer, The oxidation state of dispersed Rh on Al<sub>2</sub>O<sub>3</sub>, *J. Chem. Phys.* 74 (1981) 6487–6497, <https://doi.org/10.1063/1.440987>.
- [48] E. Varga, P. Pusztai, L. Óvári, A. Oszkó, A. Erdöhelyi, C. Papp, H.P. Steinrück, Z. Kónya, J. Kiss, Probing the interaction of Rh, Co and bimetallic Rh-Co nanoparticles with the CeO<sub>2</sub> support: catalytic materials for alternative energy generation, *Phys. Chem. Chem. Phys.* 17 (2015) 27154–27166, <https://doi.org/10.1039/C5CP03549J>.
- [49] M. Marwood, R. Doepper, A. Renken, In-situ surface and gas phase analysis for kinetic studies under transient conditions The catalytic hydrogenation of CO<sub>2</sub>, *Appl. Catal. A* 151 (1997) 223–246, [https://doi.org/10.1016/S0926-860X\(96\)00267-0](https://doi.org/10.1016/S0926-860X(96)00267-0).
- [50] L. Falbo, C.G. Visconti, L. Lietti, J. Szanyi, The effect of CO on CO<sub>2</sub> methanation over Ru/Al<sub>2</sub>O<sub>3</sub> catalysts: a combined steady-state reactivity and transient DRIFT spectroscopy study, *Appl. Catal. B* 256 (2019), 117791, <https://doi.org/10.1016/j.apcatb.2019.117791>.
- [51] K.K. Bando, K. Soga, K. Kunimori, H. Arakawa, Effect of Li additive on CO<sub>2</sub> hydrogenation reactivity of zeolite supported Rh catalysts, *Appl. Catal. A* 175 (1998) 67–81, [https://doi.org/10.1016/S0926-860X\(98\)00202-6](https://doi.org/10.1016/S0926-860X(98)00202-6).
- [52] C. Wang, E. Guan, L. Zhang, X. Chu, Z. Wu, J. Zhang, Z. Yang, Y. Jiang, L. Zhang, X. Meng, B.C. Gates, F.S. Xiao, Product Selectivity Controlled by Nanoporous Environments in Zeolite Crystals Enveloping Rhodium Nanoparticle Catalysts for CO<sub>2</sub> Hydrogenation, *J. Am. Chem. Soc.* 141 (2019) 8482–8488, <https://doi.org/10.1021/jacs.9b01555>.
- [53] H. Hendrickx, A. Jongenelis, B.E. Nieuwenhuys, Adsorption and dissociation of carbon dioxide on rhodium surfaces, *Surf. Sci.* 154 (1985) 503–523, [https://doi.org/10.1016/0039-6028\(85\)90047-0](https://doi.org/10.1016/0039-6028(85)90047-0).
- [54] B. Bartos, H.J. Freund, H. Kühlenbeck, M. Neumann, H. Lindner, K. Müller, Adsorption and reaction of CO<sub>2</sub> and CO<sub>2</sub>/O CO-adsorption on Ni(110): Angle resolved photoemission (ARUPS) and electron energy loss (HREELS) studies, *Surf. Sci.* 179 (1987) 59–89, [https://doi.org/10.1016/0039-6028\(87\)90120-8](https://doi.org/10.1016/0039-6028(87)90120-8).
- [55] M. Pachecka, J.M. Sturm, C.J. Lee, F. Bijkker, Adsorption and Dissociation of CO<sub>2</sub> on Ru(0001), *J. Phys. Chem. C* 121 (2017) 6729–6735, <https://doi.org/10.1021/acs.jpcc.7b00021>.
- [56] D.W. Goodman, D.E. Peebles, J.M. White, CO<sub>2</sub> dissociation on rhodium: measurement of the specific rates on Rh(111), *Surf. Sci.* 140 (1984) L239–L243, [https://doi.org/10.1016/0167-2584\(84\)90153-1](https://doi.org/10.1016/0167-2584(84)90153-1).
- [57] F. Solymosi, The bonding, structure and reactions of CO<sub>2</sub> adsorbed on clean and promoted metal surfaces, *J. Mol. Catal.* 65 (1991) 337–358, [https://doi.org/10.1016/0304-5102\(91\)85070-1](https://doi.org/10.1016/0304-5102(91)85070-1).
- [58] S.G. Wang, D.B. Cao, Y.W. Li, J. Wang, H. Jiao, Chemisorption of CO<sub>2</sub> on Nickel Surfaces, *J. Phys. Chem. B* 109 (2005) 18956–18963, <https://doi.org/10.1021/jp052355g>.
- [59] E. Vesselli, L. De Rogatis, X. Ding, A. Baraldi, L. Savio, L. Vattuone, M. Rocca, P. Fornasiero, M. Peressi, A. Baldereschi, R. Rosei, G. Comelli, Carbon Dioxide

- Hydrogenation on Ni(110), *J. Am. Chem. Soc.* 130 (2008) 11417–11422, <https://doi.org/10.1021/ja802554g>.
- [60] F. Ouyang, J.N. Kondo, K.I. Maruya, K. Domen, Site Conversion of Methoxy Species on  $\text{ZrO}_2$ , *J. Phys. Chem. C* 101 (1997) 4867–4869, <https://doi.org/10.1021/jp971048a>.
- [61] I.A. Fisher, A.T. Bell, In Situ Infrared Study of Methanol Synthesis from  $\text{H}_2/\text{CO}$  over  $\text{Cu}/\text{SiO}_2$  and  $\text{Cu}/\text{ZrO}_2/\text{SiO}_2$ , *J. Catal.* 178 (1998) 153–173, <https://doi.org/10.1006/jcat.1998.2134>.
- [62] J.A. Anderson, M.M. Khader, A high pressure, high temperature infrared study of CO hydrogenation over  $\text{Rh}/\text{ZrO}_2$ , *J. Mol. Catal. A* 105 (1996) 175–183, [https://doi.org/10.1016/1381-1169\(95\)00247-2](https://doi.org/10.1016/1381-1169(95)00247-2).
- [63] M.D. Rhodes, K.A. Pokrovski, A.T. Bell, The effects of zirconia morphology on methanol synthesis from CO and  $\text{H}_2$  over  $\text{Cu}/\text{ZrO}_2$  catalysts: Part II. Transient-response infrared studies, *J. Catal.* 233 (2005) 210–220, <https://doi.org/10.1016/j.jcat.2005.04.027>.
- [64] D. Bianchi, T. Chafik, M. Khalfallah, S.J. Teichner, Intermediate species on zirconia supported methanol aerogel catalysts: II. Adsorption of carbon monoxide on pure zirconia and on zirconia containing zinc oxide, *Appl. Catal. A* 105 (1993) 223–249, [https://doi.org/10.1016/0926-860X\(93\)80250-T](https://doi.org/10.1016/0926-860X(93)80250-T).
- [65] S. Bernal, J.J. Calvino, G.A. Cifredo, A. Laachir, V. Perrichon, J.M. Herrmann, Influence of the Reduction/Evacuation Conditions on the Rate of Hydrogen Spillover on  $\text{Rh}/\text{CeO}_2$  Catalysts, *Langmuir* 10 (1994) 717–722, <https://doi.org/10.1021/la00015a020>.
- [66] D. Panayotov, M. Mihaylov, D. Nihtianova, T. Spasovc, K. Hadjiivanov, Spectral evidence for hydrogen-induced reversible segregation of CO adsorbed on titania-supported rhodium, *Phys. Chem. Chem. Phys.* 16 (2014) 13136–13144, <https://doi.org/10.1039/C4CP01136H>.
- [67] L.E. Depero, R. Bertocello, T. Boni, P. Levring, I.N. Sora, E. Tempesti, F. Parmigiani, Surface and bulk characterization of  $\text{Rh}/\text{ZrO}_2$  prepared by absorption of  $\text{Rh}_4(\text{CO})_{12}$  clusters on  $\text{ZrO}_2$  powder, *J. Mater. Res.* 12 (1997) 1376–1384, <https://doi.org/10.1557/JMR.1997.0187>.
- [68] T. Tabakova, F. Boccuzzi, M. Manzoli, D. Andreeva, FTIR study of low-temperature water-gas shift reaction on gold/ceria catalyst, *Appl. Catal. A* 252 (2003) 385–397, [https://doi.org/10.1016/S0926-860X\(03\)00493-9](https://doi.org/10.1016/S0926-860X(03)00493-9).
- [69] C.M. Kalamaras, S. Americanou, A.M. Efstathiou, “Redox” vs “associative formate with –OH group regeneration” WGS reaction mechanism on  $\text{Pt}/\text{CeO}_2$ : Effect of platinum particle size, *J. Catal.* 279 (2011) 287–300, <https://doi.org/10.1016/j.jcat.2011.01.024>.
- [70] L.F. Bobadilla, V. Garcilaso, M.A. Centeno, J.A. Odriozola, Monitoring the Reaction Mechanism in Model Biogas Reforming by In Situ Transient and Steady-State DRIFTS Measurements, *ChemSusChem* 10 (2017) 1193–1201, <https://doi.org/10.1002/cssc.201601379>.
- [71] M. Escobar, F. Gracia, A. Karelavic, R. Jiménez, Kinetic and in situ FTIR study of CO methanation on a  $\text{Rh}/\text{Al}_2\text{O}_3$  catalyst, *Catal. Sci. Technol.* 5 (2015) 4532–4541, <https://doi.org/10.1039/C5CY00676G>.
- [72] G. Lafaye, C. Mihut, C. Especel, P. Marécot, M.D. Amiridis, FTIR Studies of CO Adsorption on  $\text{Rh}-\text{Ge}/\text{Al}_2\text{O}_3$  Catalysts Prepared by Surface Redox Reactions, *Langmuir* 20 (2004) 10612–10616, <https://doi.org/10.1021/la049692l>.
- [73] C. Schild, A. Wokaun, R.A. Koepfel, A. Baiker, Carbon dioxide hydrogenation over nickel/zirconia catalysts from amorphous precursors: on the mechanism of methane formation, *J. Phys. Chem.* 95 (1991) 6341–6346, <https://doi.org/10.1021/j100169a049>.
- [74] G. Zhou, H. Liu, K. Cui, A. Jia, G. Hu, Z. Jiao, Y. Liu, X. Zhang, Role of surface Ni and Ce species of  $\text{Ni}/\text{CeO}_2$  catalyst in  $\text{CO}_2$  methanation, *Appl. Surf. Sci.* 383 (2016) 248–252, <https://doi.org/10.1016/j.apsusc.2016.04.180>.
- [75] L. Basini, M. Marchionna, A. Aragno, Drift and mass spectroscopic studies on the reactivity of rhodium clusters at the surface of polycrystalline oxides, *J. Phys. Chem.* 96 (1992) 9431–9441, <https://doi.org/10.1021/j100202a068>.
- [76] E.E. Ortelli, J.M. Weigel, A. Wokaun, Methanol synthesis pathway over  $\text{Cu}/\text{ZrO}_2$  catalysts: a time-resolved DRIFT  $^{13}\text{C}$ -labelling experiment, *Catal. Lett.* 54 (1998) 41–48, <https://doi.org/10.1023/A:1019032022881>.
- [77] D. Tibiletti, F.C. Meunier, A. Goguet, D. Reid, R. Burch, M. Boaro, M. Vicario, A. Trovarelli, An investigation of possible mechanisms for the water–gas shift reaction over a  $\text{ZrO}_2$ -supported Pt catalyst, *J. Catal.* 244 (2006) 183–191, <https://doi.org/10.1016/j.jcat.2006.09.004>.
- [78] L. Kieu, P. Boyd, H. Idriss, Modelling of the adsorption of formic acid and formaldehyde over rutile  $\text{TiO}_2(1\ 1\ 0)$  and  $\text{TiO}_2(0\ 1\ 1)$  clusters, *J. Mol. Catal. A* 176 (2001) 117–125, [https://doi.org/10.1016/S1381-1169\(01\)00231-X](https://doi.org/10.1016/S1381-1169(01)00231-X).
- [79] F. Conti, A. Hanss, C. Fischer, G. Elger, Thermogravimetric investigation on the interaction of formic acid with solder joint materials, *N. J. Chem.* 40 (2016) 10482–10487, <https://doi.org/10.1039/C6NJ02396G>.
- [80] A.K. Singh, S. Singh, A. Kumar, Hydrogen energy future with formic acid: a renewable chemical hydrogen storage system, *Catal. Sci. Technol.* 6 (2016) 12–40, <https://doi.org/10.1039/C5CY01276G>.
- [81] M.W. Balakos, S.S.C. Chuang, G. Srivas, Transient Infrared Study of Methanation and Ethylene Hydroformylation over  $\text{Rh}/\text{SiO}_2$  Catalysts, *J. Catal.* 140 (1993) 281–285, <https://doi.org/10.1006/jcat.1993.1083>.
- [82] M. Zhou, L. Andrews, Reactions of Laser-Ablated Co, Rh, and Ir with CO: Infrared Spectra and Density Functional Calculations of the Metal Carbonyl Molecules, Cations and Anions in Solid Neon, *J. Phys. Chem. A* 103 (1999) 7773–7784, <https://doi.org/10.1021/jp991400f>.
- [83] J.J. Benítez, R. Alvero, M.J. Capitan, I. Carrizosa, J.A. Odriozola, DRIFTS study of adsorbed formate species in the carbon dioxide and hydrogen reaction over rhodium catalysts, *Appl. Catal.* 71 (1991) 219–231, [https://doi.org/10.1016/0166-9834\(91\)85081-6](https://doi.org/10.1016/0166-9834(91)85081-6).
- [84] M. Dang-Nhu, A.S. Pine, A.G. Robiette, Spectral intensities in the  $\nu_3$  bands of  $^{12}\text{CH}_4$  and  $^{13}\text{CH}_4$ , *J. Mol. Spectrosc.* 77 (1979) 57–68, [https://doi.org/10.1016/0022-2852\(79\)90196-6](https://doi.org/10.1016/0022-2852(79)90196-6).
- [85] N.M. Gupta, V.S. Kamble, R.M. Iyer, K.R. Thampi, M. Gratzel, FTIR studies on the CO,  $\text{CO}_2$  and  $\text{H}_2$  co-adsorption over  $\text{Ru}-\text{RuO}_x/\text{TiO}_2$  catalyst, *Catal. Lett.* 21 (1993) 245–255, <https://doi.org/10.1007/BF00769476>.
- [86] C. Liu, J.M. Notestein, E. Weitz, K.A. Gray, Photo-Initiated Reduction of  $\text{CO}_2$  by  $\text{H}_2$  on Silica Surface, *ChemSusChem* 11 (2018) 1163–1168, <https://doi.org/10.1002/cssc.201702341>.
- [87] M.A. Henderson, S.D. Worley, An infrared study of the hydrogenation of carbon dioxide on supported rhodium catalysts, *J. Phys. Chem.* 89 (1985) 1417–1423, <https://doi.org/10.1021/j100254a023>.
- [88] J.J. Benítez, R. Alvero, I. Carrizosa, J.A. Odriozola, “In situ” drifts study of adsorbed species in the hydrogenation of carbon oxides, *Catal. Today* 9 (1991) 53–60, [https://doi.org/10.1016/0920-5861\(91\)85007-U](https://doi.org/10.1016/0920-5861(91)85007-U).
- [89] Z. Hao, J. Shen, S. Lin, X. Han, X. Chang, J. Liu, M. Li, X. Ma, Decoupling the effect of Ni particle size and surface oxygen deficiencies in  $\text{CO}_2$  methanation over ceria supported Ni, *Appl. Catal. B. Environ.* 286 (2021), 119922, <https://doi.org/10.1016/j.apcatb.2021.119922>.
- [90] R.-P. Ye, Q. Li, W. Gong, T. Wang, J.J. Razink, L. Lin, Y.-Y. Qin, Z. Zhou, H. Adidharm, J. Tang, A.G. Russell, Y.-G. Ma, Fan, Yao, High-performance of nanostructured  $\text{Ni}/\text{CeO}_2$  catalyst on  $\text{CO}_2$  methanation, in: *Appl. Catal. B. Environ.* 286, 2020, 118474, <https://doi.org/10.1016/j.apcatb.2019.118474>.
- [91] H. Chen, P. Liu, J. Liu, X. Feng, S. Zhou, Mechanochemical in-situ incorporation of Ni on  $\text{MgO}/\text{MgH}_2$  surface for the selective O-/C-terminal catalytic hydrogenation of  $\text{CO}_2$  to  $\text{CH}_4$ , *J. Catal.* 394 (2021) 397–405, <https://doi.org/10.1016/j.jcat.2020.10.026>.